1-23-1989

# The 157 nm Photodissociation of OCS

C. E. Strauss
*Cornell University*

George C. McBane
*Grand Valley State University*, mcbaneg@gvsu.edu

P. L. Houston
*Cornell University*

I. Burak
*Tel Aviv University*

J. W. Hepburn
*University of Waterloo*

# The 157 nm photodissociation of OCS

C. E. Strauss, G. C. McBane, and P. L. Houston
*Department of Chemistry, Cornell University, Ithaca, New York 14853-1302*

I. Burak
*School of Chemistry, Tel Aviv University, Tel Aviv, Israel*

J. W. Hepburn[a)]
*Department of Chemistry, University of Waterloo, Waterloo, Ontario, Canada*

(Received 13 December 1988; accepted 23 January 1989)

The photodissociation of OCS at 157 nm has been investigated by using tunable vacuum ultraviolet radiation to probe the CO and S photoproducts. Sulfur is produced almost entirely in the $^1S$ state, while CO is produced in its ground electronic state and in vibrational levels from $v = 0$–3 in the approximate ratio $(v = 0):(v = 1):(v = 2):(v = 3) = (1.0):(1.0):(0.5):(0.3)$. The rotational distribution for each vibrational level is found to be near Boltzmann, with temperatures that decrease from 1350 K for $v = 0$ to 780 K for $v = 3$. Measurements of the CO Doppler profiles demonstrate that the dissociation takes place from a transition of predominantly parallel character ($\beta = 1.8 \pm 0.2$) and that the CO velocity and angular momentum vectors are perpendicular to one another.

## I. INTRODUCTION

The dynamics of molecular photodissociation have been investigated intensively during the past decade,[1–7] in part because laser-based techniques have made it possible to dissociate the parent molecules and to probe the fragments with energy and state resolution and in part because the dissociative event, which begins from a restricted range of geometries, is simpler to model than a collisional event, where it is very difficult to control the impact parameter and orientation of the colliding fragments. Studies of the dissociation of triatomic molecules have been particularly fruitful.[5–7] A formal theory of such photodissociations has been developed,[8] and both theoretical and experimental studies have probed several important systems. Recent developments concerning the correlation between vector properties in the dissociation promise to provide even more detail than had previously been realized.[9–12]

The photodissociation dynamics of the isoelectronic molecules $CO_2$, OCS, and $CS_2$ form an attractive target for investigation. The spectroscopy of these molecules has been studied extensively[6,13] and shows that they may be excited by absorption to electronic states of either linear or bent equilibrium geometries. Sufficiently intense laser sources have recently become available for photodissociation studies in the vacuum ultraviolet.[14,15] The CO, CS, O, and S fragments can all be probed sensitively, either by laser-induced fluorescence (LIF) or by multiphoton ionization (MPI).[16–20] In the cases of OCS and $CS_2$ the heavy S atom contribution makes it possible to study the participation of triplet states in the dissociation process, reached either by direct absorption or by curve crossing from a singlet state. Results from our research program concerning the photodissociation of $CS_2$ at 193 nm (Ref. 21) and of OCS near 222 nm (Refs. 10, 22, and 23) have been presented previously, and a report on the photodissociation of $CO_2$ at 157 nm is forthcoming.[24] This paper concerns the photodissociation of OCS at 157 nm.

A detailed discussion of the OCS electronic spectroscopy has been given by Rabalais *et al.*,[13] who provided the following assignments:

$^1\Delta \leftarrow {}^1\Sigma$, $\lambda = 222.3$ nm,

$^1\Pi \leftarrow {}^1\Sigma$, $\lambda = 166.7$ nm,

$^1\Sigma \leftarrow {}^1\Sigma$, $\lambda = 152.3$ nm.

The photodissociation of OCS has been examined by several investigators, particularly at wavelengths near 222 nm. The increase in the OCS absorption coefficient with temperature has been used by four groups in assigning the geometry of the upper state to a bent configuration.[25–28] Zittel and his co-workers[29,30] have exploited this effect in the two-step photodissociation of OCS to separate O, C, and S isotopes. More recently, detailed product state distributions and vector correlations[10,22,23] have shown that absorption takes place to two surfaces of $A'$ and $A''$ symmetry derived from a bent $^1\Delta$ configuration. The sole sulfur product appears to be $S(^1D)$, in agreement with a previous measurement.[31] The CO photofragment is produced almost exclusively in $v = 0$, but the rotational distribution is inverted and peaked at very high rotational levels.

The dissociation from the excited $^1\Sigma$ state has been previously investigated using the 157 nm radiation of the $F_2$ laser. Photolysis at 157 nm can produce the following products:

$$\begin{aligned} OCS + 157\text{ nm} &\rightarrow CO(^1\Sigma) + S(^3P) + 38\,290\text{ cm}^{-1} \\ &\rightarrow CO(^1\Sigma) + S(^1D) + 29\,060\text{ cm}^{-1} \\ &\rightarrow CO(^1\Sigma) + S(^1S) + 16\,110\text{ cm}^{-1} \\ &\rightarrow CS(^1\Sigma) + O(^3P) + 8500\text{ cm}^{-1}. \end{aligned}$$

Black and Sharpless[32,33] have studied the emission from the $^1S$ metastable state of the sulfur atom. A quantum yield of $0.80 \pm 0.05$ has been determined for the $S(^1S)$ formation in the 157 nm dissociation. Ondrey *et al.* performed time-of-

[a)] Alfred P. Sloan Foundation Fellow.

 0021-9606/89/105364-09$02.10 

flight measurements on the S-atom product and interpreted them to indicate that the CO vibrational distribution was highly inverted, with a peak in the vibrational distribution at the $v = 5$ level and progressively less population in lower levels.[34]

The use of tunable coherent vacuum ultraviolet (VUV) makes extremely sensitive, state-selective detection of CO and S possible using LIF.[18] The goal of this work was to use the LIF method to obtain detailed information about the CO internal state distribution, about the electronic state distribution of the sulfur atom, and about the vector correlations characterizing the dissociation process. In contrast to the previous time-of-flight measurements, we find relatively little energy disposal into the CO vibrational degree of freedom. Much of the available energy goes into relative recoil and into the electronic excitation of S($^1$S), which appears to be the major sulfur product produced in the dissociation. The amount of rotational excitation found in the CO photofragment indicates that the dissociation mechanism is not consistent with fragmentation on an excited surface of linear geometry. Measurement of the Doppler profiles of selected CO vibrational–rotational transitions indicates that the recoil and CO angular momentum vectors are perpendicular, as expected from conservation of angular momentum, that the dissociation is rapid compared to parent rotation, and that the absorption transition in the OCS parent is via a parallel transition, with the anisotropy parameter measured to be $\beta = 1.8 \pm 0.2$.

## II. EXPERIMENTAL

### A. Molecular beam chamber

Sample concentrations of 10%, 5%, 2%, and 0.5% OCS seeded in helium at 1.7 atm. stagnation pressure were supersonically expanded through a pulsed beam valve (Newport BV-100) with a 0.5 mm orifice into a background chamber pressure of roughly $5 \times 10^{-5}$ torr. Although there was no convenient method for determining the rotational temperature of the OCS in the jet, a 1:35 mixture of CO in He under the same nozzle conditions was found to have a 3 K rotational temperature.

The photolysis beam, the probe beam, and the molecular beam propagated along mutually orthogonal directions, intersecting about 20–30 nozzle diameters downstream of the orifice. Both laser beams entered the chamber through long arms equipped with irises to minimize scattered light. The entrance windows were nonbirefringent LiF flats mounted perpendicular to the propagation directions to preserve light polarizations. Laser-induced fluorescence (LIF) was collected through a LiF window at 45° to both laser beams using a single F/1 lens ($MgF_2$). Stops restricted the viewing region to approximately 4–5 mm in diameter.

### B. Probe laser

Laser induced fluorescence was used to probe the vibrational and rotational populations of the CO product on the $A\,^1\Pi \leftarrow X\,^1\Sigma^+$ system and to probe the sulfur ($^1$S, $^1$D, $^3$P) products on a variety of atomic transitions. The VUV required for these measurements was generated by two-photon resonantly enhanced four-wave sum mixing in magnesium vapor,[18] a technique which has been used by our groups in several experiments.[21–24] The oscillator and amplifier sides of a twin-cavity XeCl excimer laser (Lambda Physik EMG 150ES) were configured as two synchronized oscillators to pump two dye lasers (Lambda Physik FL-2002E). For each dye laser the pulse duration and linewidth were approximately 10 ns and 0.25 cm$^{-1}$ full width at half maximum (FWHM), respectively; each polarization was vertical. For CO detection, one of the dye lasers was fixed at 430.9 nm, which corresponds to the $3s3d\ ^1\mathrm{D} \leftarrow 3s^2\ ^1\mathrm{S}$ two-photon resonance in Mg, and the other dye laser could be tuned across the visible spectrum to generate VUV between 140 and 170 nm. To generate the 168.75 nm necessary for S($^1$S) detection, the $3s4s\ ^1\mathrm{S} \leftarrow 3s^2\ ^1\mathrm{S}$ two-photon resonance in Mg was used, with the fixed wavelength dye laser at 459.7 nm. The dye laser pulse energies were typically 5 mJ/pulse for the fixed wavelength laser and 15 mJ/pulse for the tunable laser.

The laser beams were temporally overlapped by a 16 ns optical delay path on the fixed frequency laser. A $\lambda/2$ plate rotated by 90° the polarization of one of the two laser beams. The beams were then spatially overlapped using a Glan–Taylor prism, which combined the beams without appreciable loss and acted as a clean-up polarizer. Following the prism, a $\lambda/4$ plate was used to convert each beam to circular polarization in order to enhance the sum frequency generation over the frequency tripling of the fixed frequency laser. The VUV output was nominally circularly polarized.

A 25 cm focal length quartz lens focused the beams into the magnesium oven, and the VUV was recollimated by a 38 cm focal length. $MgF_2$ lens placed after the oven. The fundamental frequencies together with the VUV were transmitted through the beam chamber. The VUV was monitored by a solar-blind photomultiplier tube (EMI G-26E314LF) by taking a reflection from a quartz window at 45° to the probe beam, and by passing it through a $MgF_2$ diffuser and a VUV bandpass filter (Acton 140-B) directly onto the photocathode. The filter response varied less than 3% over the wavelength region of the experiment, and no correction was made for this effect. The VUV was transmitted through about 2 meters of argon-purged or evacuated tube before reaching the molecular beam chamber.

To record Doppler profiles, intracavity air-spaced etalons were used in both dye lasers to narrow the bandwidths to about 0.05 cm$^{-1}$. The tunable dye laser was scanned under computer control by using a variable pressure of $N_2$ in the dye laser oscillator. To calibrate the linewidth of the resulting VUV, Doppler line shapes were recorded for jet-cooled CO molecules. Under the observation conditions used to detect photofragments the VUV linewidth observed was 0.22 cm$^{-1}$ FWHM.

The four-wave mixing VUV generation in magnesium has been detailed previously [18,21–23] However, a noteworthy improvement has been made since previous publications. With the addition of lithium in roughly an equal part by volume to the magnesium, crystal growth ceased and refluxing from the cooled zone improved. Previously, magnesium crystals grew in the condensation region and blocked the optical path, restricting operation of each pipe to 3–5 days

use. Our modified pipe has functioned for over a year. The absolute VUV output energy was not measured, but from spectra of CO taken at known pressures we estimate a sensitivity limit (S/N = 1) of $10^6$–$10^7$ molecules per quantum state.

### C. Photolysis laser

Unpolarized photolysis radiation at 157 nm was produced with an excimer laser (Lambda Physik, EMG-101) operating on a mix of fluorine and neon in a 3 bar helium buffer. The light output is at two closely spaced wavelengths in the vacuum ultraviolet (15% at 157.52 nm and 85% at 157.63 nm);[35,36] deep red emission (600–800 nm) is also observed. The energy output was 1–5 mJ/pulse at 50 Hz. Since 157 nm radiation is absorbed by air as well as most "reflectors," a straight optical path from the laser cavity to the molecular beam chamber was used and purged with argon. A 1-m (nominal for visible light) LiF lens focused the light; small displacements of this lens allowed a 4 mm lateral shift of the focus. The $F_2$ spot intersecting the molecular beam was rectangular with about a 4 to 1 aspect ratio; the long axis lay along the probe beam direction. Spot sizes at the intersection were 1 to 6 mm (perpendicular to probe) variable with the lens position. The laser spot sizes were measured by translating a fine wire through the laser beam in the photolysis volume and monitoring scattered light as a function of wire position using the LIF monitor photomultiplier tube (PMT) without the light collection lens to detect the scattered light. The removal of the light collection optics enlarged the field of view of the PMT.

The 157 nm light intensity was monitored by visible fluorescence induced on the nearly resonant $B'\,^2\Delta \leftarrow X\,^2\Pi$ transition in NO.[35,36] The VUV passed first through the molecular beam chamber and entered unfocused into a cell containing 400 Torr of NO. A 10 cm lens gathered fluorescence perpendicular to the laser beam direction onto a photomultiplier (Hamamatsu 1P120) after the laser had traversed a 7.5 cm path through the NO. A 555-565 nm bandpass filter and temporal discrimination allowed rejection of the scattered red laser emission and the white light from the laser discharge. During the course of the experiment, a dark, shiny, absorbing residue was burned onto the chamber photolysis input window, presumably a combination of OCS photoproducts and diffusion pump oil. To reduce this effect the aluminum input arm was packed in 6 in. of dry ice as a trap.

A critical modification of the excimer laser extended its gas-fill lifetime from about 10 000 shots to an experimentally useful range (hours to days) with periodic fluorine addition. Gas was continually cleansed of absorbing impurities (e.g., $CF_4$, $COF_2$,...) by circulation through a homebuilt gas purification unit incorporating a metal bellows pump and a liquid-nitrogen trap.

### D. Detection electronics

Fluorescence detection of the S and CO photofragments was accomplished using a solar blind photomultiplier tube (EMR 541G-09-17). Signals from all three photomultipliers were averaged for typically ten shots by gated integrators (SRS, Model No. SR250) with apertures similar in time duration to the fluorescence signals. A computer (IBM PC or DEC LSI-11) collected the digitized data and controlled the dye laser wavelength scanning. For Doppler profiles a custom-built (Quanta Ray) servo was used to ramp the nitrogen tuning pressure. For each line, many spectral scans were taken rapidly in succession without averaging and then later combined so that as many as 100 shots per point could be averaged while drifts in the photolysis laser power could be minimized.

The shortest delay between pump and probe (200 ns) was limited by the recovery time of the photomultiplier response to the scattered 157 nm light. The scatter was both from uncontrolled light paths and from the OCS itself. The shot rate was 10 Hz limited by the XeCl excimer laser. The gated integrators were triggered by a photodiode viewing the dye laser amplifier cell so that trigger jitter of the laser would not affect the gate timing.

The dominant noise source was scattered light from the photolysis laser. Both amplitude and temporal jitter caused large swings in the scattered light base line signal and the PMT recovery. A second noise source was the coherent portion of the rf noise pulse following the excimer discharge. A substantial improvement in the signal-to-noise ratio was obtained by using a 20 Hz repetition rate for the photolysis laser in conjunction with the active base line subtraction feature of the boxcar integrator.

### E. Chemicals

OCS was obtained from Matheson at a stated purity of 96%. The sample was subjected to freeze-pump-thaw cycles at liquid-$N_2$ temperatures to remove any CO present. Less volatile impurities, such as $CS_2$, were reduced by simple distillation from samples held at methanol (179 K) or ethanol (156 K) slush bath temperatures.

## III. RESULTS

### A. The relative yield of sulfur products

The relative amounts of $S(^1S)$, $S(^1D)$, and $S(^3P)$ formed in the 157-nm photodissociation of OCS were determined by comparing the strengths of the LIF signals for the corresponding atomic resonance lines $^1P \leftarrow {}^1S$ at 1688 Å, $^1P \leftarrow {}^1D$ at 1448 Å, and $^3D \leftarrow {}^3P$ at 1484 Å.[37] This comparison demonstrated that the $S(^1S)$ quantum yield was nearly unity. Some difficulty in measuring the ratio of $S(^1S)$ to $S(^1D)$ signal strengths was caused by the necessity of using different dyes to reach the two transitions and different photomultiplier bias voltages to observe the signals. Because the $S(^1D)$ line at 1448 Å and the $S(^3P)$ line at 1484 Å overlap the (3,0) and (2,0) CO bands, respectively, it was also possible to compare the $S(^1D)$ and $S(^3P)$ signals to signals from adjacent CO lines by taking into account the linestrengths of the atomic and molecular transitions and the population distribution of the CO (see below).[37,38] These more accurate measurements showed that the $S(^3P)$ and $S(^1D)$ quantum yields were less than 2% each. A possible source for the $S(^3P)$ signal is dissociation of OCS clusters. The yield of

$S(^3P)$ relative to the yield of CO dropped by a factor of 5 in going from beam to bulb conditions.

### B. CO vibrational and rotational distributions

The internal energy distribution of the $CO(X\,^1\Sigma^+)$ photofragment was determined by analyzing the LIF spectra. To probe the various CO product vibrational levels, the (0,0), (1,1), (3,2), and (5,3) bands of the $A\,^1\Pi \leftarrow X\,^1\Sigma^+$ system were recorded and analyzed. A small region of the spectrum, showing portions of the (0,0), (3,2), and (5,3) bands, is reproduced in Fig. 1. The observed spectra were normalized by the measured VUV probe laser power, and the intensities for the unperturbed rotational lines in the spectra were measured and divided by the appropriate Hönl–London factors to obtain the relative populations in the various product rotational states for each CO vibrational level. The measured population distributions based on $Q$-branch transitions are shown as Boltzmann plots in Fig. 2 for $v = 0$, 1, 2, and 3. Although there is no justification for assuming that the rotational distributions can be described by a temperature, particularly since they are the product of a system at fixed total energy, in the case of every vibrational level the $P(J)$ distribution was well represented by a straight line on the Boltzmann plot. We will use the temperatures corresponding to these lines as a convenient parameter for describing the distributions. The temperature was found to vary for the different CO vibrational levels; the full data set provided the following parameters: $v = 0$, $T_{rot} = 1350$ K; $v = 1$, $T_{rot} = 1300$ K; $v = 2$, $T_{rot} = 980$ K; and $v = 3$, $T_{rot} = 770$ K.

The CO product vibrational distribution was obtained by comparing the relative intensities for the CO ($A\,^1\Pi \leftarrow X\,^1\Sigma$) bands detected, normalizing these by the probe laser power and correcting for the detector response. These corrected relative LIF intensities were converted into overall band intensities using the known rotational temperatures in each vibrational level to calculate the integrated intensity for each band. In order to get relative vibrational populations from these data, the integrated band intensities were then

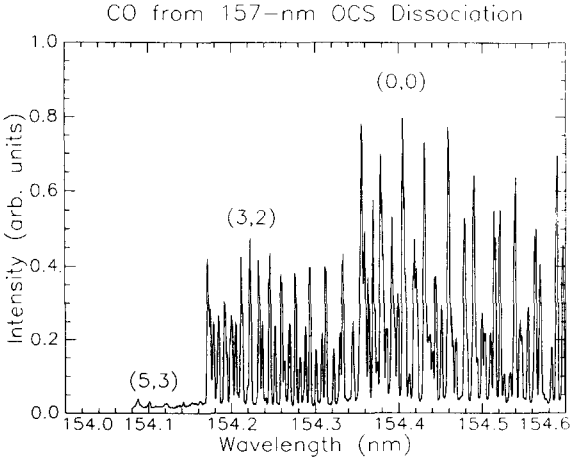


FIG. 1. Portion of the laser-induced fluorescence spectrum of CO produced in the 157-nm photodissociation of OCS showing regions of the (0,0), (3,2), and (5,3) bands.

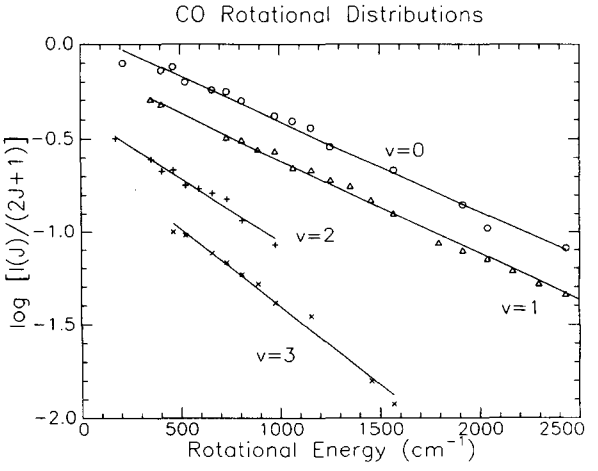


FIG. 2. Rotational distribution of the CO product of the 157-nm photodissociation of OCS based on measurements of $Q$-branch lines. The distribution is observed to be Boltzmann (solid line fits) with temperatures of 1350 K for $CO(v = 0)$, 1300 K for $CO(v = 1)$, 980 K for $CO(v = 2)$, and 770 K for $CO(v = 3)$.

divided by the appropriate Franck–Condon factors, calculated by Waller and Hepburn.[21] The relative populations found were $(v = 0):(v = 1):(v = 2):(v = 3) = (1.0):(1.0):(0.5):(0.3)$. Attempts were made to detect $v = 4$ and $v = 5$ products by recording spectra in the region of the (3,4) and (5,5) bandheads (1648 Å and 1630 Å). No signal was observed from these bands, in spite of good VUV intensity and Franck–Condon factors. From this observation we conclude that the population in $v = 4$ and $v = 5$ is less that 5% of the $v = 0$ product population.

### C. Doppler profiles of CO and S(¹S) lines

High-resolution Doppler spectra of the CO fragment were recorded for several rotational lines in the (0,0), (3,0), and (1,1) vibrational bands. Typical results are shown in Fig. 3 for the $Q(19)$ line of the (0,0) band and the $R(25)$ line of the (3,0) band. The calculated Doppler line shapes are superimposed on the data and will be discussed in Sec. IV C. Shapes qualitatively similar to that for the $Q(19)$ line were observed for a wide range of $Q$-branch transitions in all vibrational levels, and shapes similar to that for the $R(24)$ line were observed for a wide range of $P$- and $R$-branch transitions in all vibrational levels. To model the line shapes, the CO velocity was selected to correspond to the $CO(v = 0,J) + S(^1S)$ channel, and the vector correlation assumed was $v \perp J$. The data shown are best described by a $\beta$ parameter of 1.8.

## IV. DISCUSSION

### A. The quantum yield of S(¹S)

Our results demonstrate that $S(^1S)$ is the sole sulfur product of the OCS 157 nm dissociation. The absolute quantum yield for the $S(^1S)$ production was found by Black and Sharpless to be $0.80 \pm 0.05$.[32,33] Our results limit the formation of $S(^3P)$ and $S(^1D)$ species to less than 2% each. As a

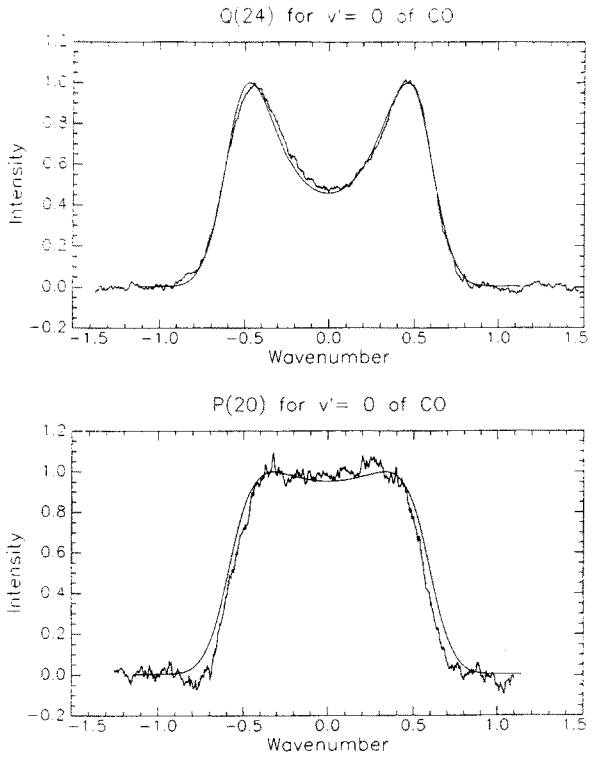


FIG. 3. Doppler profiles of the $Q(19)$ line of the (0,0) band and the $R(25)$ line of the (3,0) band of CO produced in the 157-nm photodissociation of OCS. The smooth solid lines give calculated profiles assuming that the products are $CO(v=0,J) + S(^1S)$, that $v$ and $J$ are perpendicular, and that $\beta = 1.8$.

result one may deduce that the major channel for the CO production in the 157 nm dissociation is

$$OCS \rightarrow CO + S(^1S). \quad (1)$$

This result is also confirmed by the widths of the Doppler profiles obtained for the various CO transitions. Moreover, since Black's measured the quantum yield for the total sulfur production is less than unity, one should consider the possibility of a minor formation of oxygen through the CS channel:

$$OCS \rightarrow CS + O.$$

Our detection system is insensitive to the presence of this second channel, and our results relate only to the dominant channel (1).

### B. Internal energy distribution

#### *1. Rotational distribution*

The rotational distribution of the CO fragment of 157-nm OCS dissociation can be characterized as Boltzmann for each vibrational level with a temperature which varies from 1350 K for $v = 0$ to 780 K for $v = 3$. Such high rotational temperatures cannot be predicted for a sudden dissociation from a linear state. As shown by the discussion below, sudden approximations to a dissociation from a linear state predict much lower rotational temperatures in models based on (1) an impulse approximation, (2) a Franck–Condon approximation, and (3) the "rotational reflection principle." It thus appears that either the dissociative state is nonlinear or that final state interactions cause the rotational excitation. The variation of rotational temperature with vibrational level is consistent with a statistical model: the rotational surprisal is nearly constant for all vibrational levels, so that a single dynamical constraint appears to be responsible for the distributions.

A model in which all the rotational excitation in the diatomic fragment is derived from the impulsive separation of the $S(^1S)$ and the CO is inadequate to account for the high rotational populations observed in this work, although the functional form of the distribution is adequately predicted by this model. We first consider average quantities. Assuming that both the ground $^1\Sigma$ and excited $^1\Sigma$ states are linear, the distribution of rotational energy in an impulsive model must be related to the distribution of S–CO bending angles in the ground state of the parent. From the observed rotational distribution for $CO(v=0)$ we calculate that the average rotational energy corresponds to a rotational quantum number of $J = 22$. Since the parent molecule in the molecular beam is rotationally cold, conservation of angular momentum requires that the orbital angular momentum also be characterized by a value of $L = 22\,\hbar$. Finally, with $L = \mu v_{\rm rel} b$ and $v_{\rm rel}$ equal to $4.91 \times 10^3$ m/s for the $S(^1S) + CO(v=0)$ channel, we calculate that $b = 0.19$ Å, or that the average bending angle consistent with the rotational distribution and an impulsive dissociation is 17°. This high value of the bending angle contradicts spectroscopic constants for OCS. The square of the bending wave function is calculated[39] to be reduced by a factor of $1/e$ at an angle of 7.21°, so that an average angle of 17° is clearly unreasonable. We conclude that an impulsive model in which the rotational excitation is due only to the distribution of bending angles in the ground state cannot account for the observed rotational distribution.

The same conclusion is obtained by considering a Franck–Condon model for the rotational distribution. When the angular dependence of upper potential surface is neglected, the angular momentum distribution arises solely (assuming a nonrotating parent molecule) from the bending vibrational motion of the parent triatomic molecule. Neglecting the nonisotropic part of the upper surface potential and taking into account the angular dependence of the ground and excited wave functions of the dissociating molecule, Morse and Freed calculated the rotational distribution of the diatomic fragment.[40] When the parent molecule starts in $J = 0$ and $v = 0$, a Boltzmann distribution is predicted. The effective rotational temperature is given by

$$T = B\kappa^2/(k\eta^2), \quad (3)$$

where $B$ is the rotational constant of the diatomic fragment, $k$ is the Boltzmann constant, and $\kappa$ and $\eta$ are given by

$$\kappa = \left[ \frac{r_{12}^2 r_{23}^2}{\dfrac{r_{12}^2}{m_3} + \dfrac{r_{23}^2}{m_1} + \dfrac{(r_{12}+r_{23})^2}{m_2}} \frac{\omega_{\rm bend}}{\hbar} \right]^{1/2} \quad (4)$$

and

$$\eta = (m_1 + m_2) r_{23} / [(m_1 + m_2) r_{23} + m_1 r_{12}]. \quad (5)$$

The masses and distances in these equations are defined in

Fig. 1 of Morse and Freed.[40] The $v = 0$ and $J = 0$ conditions needed for the applicability of Eq. (3) are appropriate for our experiment, since the rotational and vibrational degrees of freedom of the OCS molecules are cooled by the supersonic expansion. Applying Eq. (3) to OCS one obtains a rotational temperature of 380 K, in contrast to the temperature of 1350 K characterizing the distribution of the observed CO($v = 0$) fragments. We conclude that, although the Boltzmann form of the distribution is consistent with a Franck–Condon model, the magnitude of the temperature is not. The rotational excitation must be due to final state interactions or to a bent excited state.

Further insight into the excited potential surface on which the CO and S dissociate can be gained by examination of the rotational reflection principle.[41,42] Schinke and Engel have performed calculations on model potential surfaces for a system closely resembling OCS.[43] In their work, the reduced mass of the separating atom and diatom were taken to be that of S–CO, and the bending force constant was taken to be nearly equal to that for the ground state of OCS.[39] (Schinke and Engel use a FWHM for the bending wavefunction of 20° vs the OCS value of 14°.) The model surfaces are characterized by a parameter $\epsilon$ which is positive for linear surfaces, negative for bent surfaces, and zero if the surface is independent of bending angle. The results of their calculation show that for $\epsilon > 0$ the CO rotational distribution has its most probable rotational level at $J = 6$, as shown in Fig. 14 of their article for an available energy of 1.3 eV. By contrast, the most probable rotational level for, say, CO($v = 0$) from our measurements is $J = 22$, with only slightly lower values at higher vibrational levels. Although our available energy is nearly 2 eV, it is clear from Schinke's results that a linear ($\epsilon > 0$) surface is inconsistent with our measurement. Comparison of our results with Fig. 4 of his paper suggests that $\epsilon$ should be in the range between $-0.25$ and $-0.50$. A slightly bent dissociative surface might then be consistent with our data.

On the other hand, even rather weak final state interactions might cause the observed degree of rotational excitation. Although the rotational temperatures are high, the fraction of energy available to the CO + S($^1$S) channel deposited into rotation is only about 4%. In other presumably linear dissociations, such as ICN$\rightarrow I(^2P_{1/2})$ + CN, the fraction of available energy deposited into rotation is about 8%.[44] The variation in rotational distribution with vibrational level can be explained by a statistical model. For reactions producing an atom and a diatomic molecule, the statistically expected or "prior" distribution is given by[45,46]

$$P_0(v,j) \propto (2j+1)(E - E_v - E_j)^{1/2} \tag{6}$$

or

$$P(f_R|f_v) = (3/2)(1-g_R)^{1/2}/(1-f_v), \tag{7}$$

where $g_R \equiv f_R/(1-f_v)$. Deviations from the prior distributions may be described by a rotational surprisal parameter, $\theta_R$, defined by the observed distribution $P(j|v)$:[46]

$$P(j|v) \equiv P_0(v,j)\exp(-\theta_0 - \theta_R g_R), \tag{8}$$

where $\theta_0$ is a normalization factor. Recognition that $f_R \equiv E_R/E_{\rm tot}$ and comparison of Eq. (8) with the Boltzmann form of the data shows that $\theta_R = E_{\rm tot}(1-f_v)/kT_{\rm rot}$. A value of $E_{\rm tot} = 16\,000\ {\rm cm}^{-1}$ for the S($^1$S) channel and the observed values for $T_{\rm rot} = 1350$, 1300, 980, and 780 for $v = 0-3$, respectively, can be used to calculate that $\theta_R = 17.0$, 15.4, 17.3, and 17.9 for $v = 0-3$, respectively. The near constancy of $\theta_R$ suggests that the same, single dynamical constraint governs the rotational distribution for each of the vibrational levels and that the variation in rotational distribution is simply a result of the reduced energy available for translation and rotation as the vibrational excitation increases.

### 2. Vibrational distribution

The vibrational distribution determined from the laser-induced fluorescence spectrum after integrating over the rotational distributions to obtain band intensities and dividing by the Franck–Condon factors calculated by Waller and Hepburn[27] was $(v=0):(v=1):(v=2):(v=3) = (1.0):(1.0):(0.5):(0.3)$.

Doppler profiles of the sulfur $^1P \leftarrow {}^1S$ transition have been analyzed to obtain an independent evaluation of the vibrational distribution. The Doppler profile for this transition was calculated assuming the measured vibrational distribution $[(v=0):(v=1):(v=2):(v=3) = (1.0):(1.0):(0.5):(0.3)]$ and the rotational distribution measured for each vibrational level (shown in Fig. 2). The velocity of a S($^1$S) atom produced in coincidence with a particular internal energy level of CO is determined by conservation of energy and linear momentum:

$$v_s = ([2m_{\rm CO}/m_s(m_s+m_{\rm CO})]\{(E(h\nu) - D_0 - E_s - vh\nu_0 - B_vJ''(J''+1)\})^{1/2}, \tag{9}$$

where $E(h\nu)$ is the energy of the photon; $D_0$ is the dissociation energy, taken to be 25 164 cm$^{-1}$;[37] $E_s$ is 22 181 cm$^{-1}$ for the $^1$S channel, $\nu_0$ is the CO vibrational frequency (2143 cm$^{-1}$), and $B_v$ is the rotational constant in the CO($v$) level [1.9313 cm$^{-1}$ for CO($v=0$)]. Thus, a distribution of CO internal energy levels can be converted via Eq. (9) into a distribution of S($^1$S) velocities. Figure 4 displays the measured S($^1$S) Doppler profile and the profile calculated from

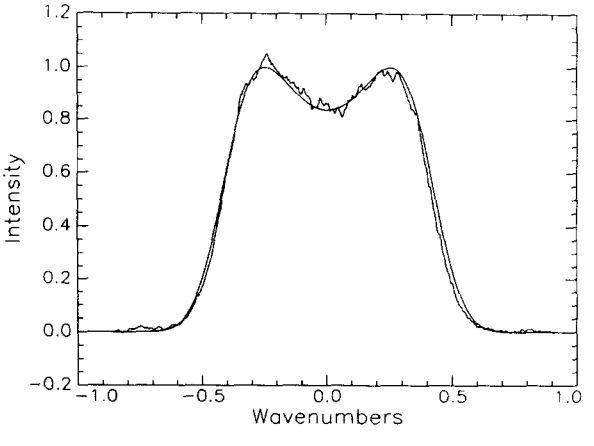


FIG. 4. Doppler profile of the S($^1$S) line with a calculated profile assuming the CO vibrational distribution given in the text.

the CO distributions. The good quantitative agreement provides independent corroboration of the measured internal energy distributions.

The vibrational distribution found in this work differs substantially from that given by Ondrey *et al.*[34] In the latter work pure OCS was expanded through a pulsed nozzle into the dissociation chamber. The molecular beam was then irradiated with pulsed light at 157 nm, and the velocity of the sulfur atom was determined by a time-of-flight technique. The high vibrational excitation of the CO fragments was inferred from the observed slow velocity distribution of the sulfur atom products. One potential problem with this work is that the authors have ignored cluster formation in cooled beams. It has been previously demonstrated that dissociation of OCS clusters results in translationally cold fragments.[23] Moreover it is expected from previous results[23] that a supersonic expansion of pure OCS results in a high degree of clustering. Indeed, following 157-nm dissociation of OCS in 10% seeded beams, we observe that all sulfur products have excess population in low translational levels when compared to dissociation of 0.5% mixtures.

The absorption profile of OCS is a broad continuum punctuated by peaks separated by roughly 800 wave numbers.[13,47] While these resonances may suggest a bound/predissociative upper state, Pack *et al.* have demonstrated that such structure can occur on simple dissociative surfaces.[48] A theoretical prediction of the vibrational distribution and absorption profile requires a complete knowledge of the excited state potential surface; such information does not exist. However, a Franck–Condon calculation which takes into account the overlap between the OCS molecular ground state wave function and that of the excited state can be performed for the cases where the ground state is modeled as two harmonic oscillators and simple upper surfaces are assumed. One possible excited state potential state wave function is simply that of the free, noninteracting fragments. A better model would place greater localization in the turning point region of the fragments' actual trajectory, where they travel the slowest and where the overlap with the ground-state wave function is the greatest. However, exact calculation of the wave function in this region can be difficult even for simple potentials. In the Morse and Freed model[40] the ground state is approximated as two harmonic oscillators in the molecular normal modes. The upper state coordinates are the free CO vibration and the center of mass separation of the fragments: the CO vibration is treated as a harmonic oscillator while, for computational feasibility, the fragment interaction potential is linearized about the turning point. This linearization gives rise to Airy wave functions. The linearization need only be valid over the integral overlap region. Exponential repulsive surfaces are popular model surfaces.[43] On such a surface we obtained a distribution in reasonable agreement with observation: $(v=0):(v=1):(v=2):(v=3) = (1.0):(1.0):(0.6):(0.17)$. In this calculation the C–O bond distances of the CO and OCS molecules were taken at their natural ground-state lengths of 1.128 A and 1.160 A, respectively, while the exponential approximation to the excited state surface was characterized by a slope of $-0.0025$ erg/cm at the OCS ground-state geometry and a range coefficient of 1.2 Bohr$^{-1}$. In general, increasing the slope parameter shifts the absorption to higher frequency and broadens the absorption linewidth; it also increases the width of the vibrational distribution. The potential we have used overestimates the OCS absorption bandwidth: the actual region over which absorption occurs is about 25% of the predicted one. However, it is expected that inclusion of rotational and translational partitioning would shrink the contribution to the width caused by the higher vibrational levels. In summary, we have sampled the upper state surface in a narrow region about 157 nm and successfully modeled it locally as an exponential repulsion. Although this potential provides a fit to the vibrational distribution, it is clear that the global potential cannot be simply repulsive; the overall width and peaked features of the absorption indicate that the potential is more complicated.

In contrast with the present results, no vibrational excitation is found in the CO photoproduct resulting from excitation of the first excited $^1\Delta$ state.[23] In this case the energy available for the nuclear motion is comparable to that available in the 157 nm dissociation, where vibrational excitation of the molecular fragment is observed. This different behavior is due to the torque exerted on the CO when the OCS molecule is excited to the highly bent $\Delta$ state. As a result of this torque, 50% of the available energy is deposited into the CO rotational degree of freedom, resulting in a highly inverted rotational distribution.[23]

### C. Vector correlations

Calculated and observed Doppler profiles of the $Q(19)$ line and the $R(25)$ line of the CO($v=0$) recorded following 157-nm photolysis of a 0.5% mixture of OCS in helium are displayed in Fig. 3. Reasonable agreement is obtained if the vector correlation between **v** and **J** is assumed to be a perpendicular one, if the recoil anisotropy is assumed to be described by $\beta = 1.8 \pm 0.2$, and if the CO($v=0, J=19$) or ($v=0, J=25$) velocity is assumed to be that which would be produced for dissociation in coincidence with a S($^1$S) sibling photofragment. The magnitude of the velocity **v**, of a particular CO($v,J$) level can be determined by conservation of energy and linear momentum:

$$v_{\mathrm{CO}}(0,J'') = \{[2m_s/m_{\mathrm{CO}}(m_s+m_{\mathrm{CO}})]\{[E(h\nu) - D_0 - E_s - BJ''(J''+1)]\}\}^{1/2}, \qquad (10)$$

where $E(h\nu)$ is the energy of the photon; $D_0$ is the dissociation energy, taken to be 25 164 cm$^{-1}$;[37] $E_s$ is 22 181 cm$^{-1}$ for the $^1$S channel; and $B = 1.9313$ cm$^{-1}$ is the rotational constant in the $v=0$ level of CO. That the dip in the $Q(19)$ line appears rather more shallow than might be expected for a value of $\beta = 1.8$ is a consequence of the fact that the $F_2$ laser is unpolarized in the plane perpendicular to its propagation direction. This lack of polarization, which decreases the Doppler profile modulation by a factor of 4, has been included in our analysis.

CO Doppler profiles obtained from this photodissociation can be influenced by at least three experimental artifacts: dissociation of clusters, reduced detectivity because of molecular motion on the time scale of detection, and satura-

tion of the dissociation. Our attempts to evaluate these factors are described below.

We know from our previous work at 222 nm that OCS expansions can produce dimers and higher clusters.[23] Profiles obtained following the 157-nm dissociation of a beam of 10% OCS in helium showed that all transitions had excess intensity in the center of the Doppler profile, which we attribute to slower fragments produced in the dissociation of clusters. This feature was reduced in 5% mixtures and was absent in mixtures containing less than 2% OCS.

A second artifact appeared even for the more dilute mixtures when highly focused pump and probe beams were employed: the intensity in the center of all transitions was somewhat reduced. We attribute this effect to the rapid motion of CO fragments out of the probe beam on the time scale of the detection, about 100 ns. Use of larger pump, probe, and detection volumes eliminated this effect.

A third possible problem is that the $F_2$ laser may saturate the OCS dissociation so that the initial alignment is less polarized than that expected in the weak field limit. We verified that the CO and S atom LIF signals were linear in $F_2$ laser power by using the $F_2$-induced NO fluorescence as a measure of the intensity at 157 nm. Thus, the value of $\beta = 1.8 \pm 0.2$ appears to be the correct one.

McCarthy and Vaida have examined the absorption spectrum of jet-cooled OCS in the region from 140-160 nm and have assigned the feature at 156.2 nm to absorption to a $^1\Pi$ electronic state.[47] According to their interpretation, the features in the vicinity of 157 nm are not consistent with the Franck–Condon envelope of a single transition connecting the $^1\Sigma^+$ ground state to the $^1\Sigma^+$ excited state. Our measurement of $\beta = 1.8 \pm 0.2$ indicates, however, that the transition at 157 nm is predominantly a parallel transition. If the upper state is linear, then absorption to the $^1\Pi$ component can be ruled out, since substantial oscillator strength to a $^1\Pi$ state at this wavelength would greatly reduce the measured value of $\beta$. In the limit of a pure $^1\Sigma^+ \rightarrow {}^1\Pi$ transition, we should have found a value for $\beta = -1.0$. However, if the upper state is appreciably bent, absorption to the $A'$ Renner–Teller component of what would have been a $^1\Pi$ state in the linear configuration might still be consistent with the high value of $\beta$ measured in this work.

Our measurement of the **v**-**J** correlation is obtained from the difference between the *Q*- and *P*- or *R*-branch transitions,[9–12] and indicates clearly that there is a perpendicular correlation, consistent with angular momentum conservation. Since the angular momenta of the parent compound and the photon are all quite small compared to the angular momentum of the CO, conservation requires that $\mathbf{J} = -\mathbf{L}$, where $\mathbf{L} = \mu(\mathbf{v} \times \mathbf{b})$, is the orbital angular momentum of the half-collision. Since **L** is perpendicular to **v**, we conclude that **J** must also be perpendicular to **v**.

## V. CONCLUSIONS

The photodissociation of OCS at 157 nm has been investigated by using laser-induced fluorescence to probe the CO and S photoproducts. More than half of the 38 290 $cm^{-1}$ of the available energy for the products is utilized for the 22 181 $cm^{-1}$ excitation of the S($^1$S) state. This leaves 16 110 $cm^{-1}$ of available energy for the nuclear degrees of freedom. About 2065 $cm^{-1}$ or 12% of this energy is allocated to vibrational excitation, while another 665 $cm^{-1}$ or 4% produces rotational excitation of the CO. About 84% of the energy available to the nuclear motion is allocated to the relative translational recoil. Rotational distributions are found to be Boltzmann for each vibrational level, and the variation in rotational temperature among the vibrational levels can be predicted by a statistical model. Dissociation of OCS at this wavelength is prompt compared to rotational motion of the parent compound, and the transition dipole moment of the OCS is aligned very nearly along the linear framework. The vector describing CO rotational motion is aligned perpendicular to the recoil velocity, as expected from conservation of angular momentum.

## ACKNOWLEDGMENTS

The authors are grateful to Professor R. D. Levine for useful discussions concerning the application of information theory to this dissociation, to Professor V. Vaida for making available a preprint of Ref. 47, to Dr. M. McCarthy for helpful discussions of this reference, and to Dr. S. Kable and Dr. G. E. Hall for assistance in obtaining some of the data. J.W.H. gratefully acknowledges NSERC Canada for financial support. This work was supported by the AFOSR under Grant No. AFOSR-860017.

[1] J. P. Simons, in *Gas Kinetics and Energy Transfer*, edited by P. G. Ashmore and R. J. Donovan (Burlington, London, 1977).
[2] H. Okabe, *Photochemistry of Small Molecules* (Wiley, New York, 1978).
[3] S. R. Leone, Adv. Chem. Phys. **50**, 255 (1982).
[4] *Molecular Photodissociation Dynamics*, edited by M. N. R. Ashfold and J. E. Baggott (Royal Society of Chemistry, London, 1987).
[5] M. Shapiro and R. Bersohn, Ann. Rev. Phys. Chem. **33**, 409 (1982).
[6] M. N. R. Ashfold, M. T. Macpherson, and J. P. Simons, Top. in Curr. Chem. **86**, 1 (1979).
[7] R. Bersohn, J. Phys. Chem. **88**, 5145 (1984).
[8] G. G. Balint-Kurti and M. Shapiro, Chem. Phys. **61**, 137 (1981).
[9] G. E. Hall, N. Sivakumar, P. L. Houston, and I. Burak, Phys. Rev. Lett. **56**, 1671 (1986).
[10] R. N. Dixon, J. Chem. Phys. **85**, 1866 (1986).
[11] P. L. Houston, J. Phys. Chem. **91**, 5388 (1987).
[12] G. E. Hall, N. Sivakumar, D. Chawla, P. L. Houston, and I. Burak, J. Chem. Phys. **88**, 3682 (1988).
[13] J. W. Rabelais, J. M. McDonald, V. Scherr, and S. P. McGlynn, Chem. Rev. **71**, 73 (1971).
[14] H. F. Dobele, M. Rowekamp, and B. Ruckle, IEEE J. Quantum Electron. **QE-20**, 1284 (1984).
[15] J. C. White, IEEE J. Quantum Electron. **QE-20**, 185 (1984).
[16] H. Rottke and H. Zacharias, Opt. Commun. **55**, 87 (1985).
[17] G. Black and L. E. Jusinski, J. Chem. Phys. **82**, 789 (1985).
[18] J. W. Hepburn, F. J. Northrup, G. L. Ogram, J. M. Williamson, and J. C. Polanyi, Chem. Phys. Lett. **85**, 127 (1982).
[19] D. Cossart and T. Bergeman, J. Chem. Phys. **65**, 5462 (1976).
[20] J. E. M. Goldsmith, J. Chem. Phys. **78**, 1610 (1983).
[21] I. M. Waller and J. W. Hepburn, J. Chem. Phys. **87**, 3261 (1987).
[22] N. Sivakumar, I. Burak, W.-Y. Cheung, J. W. Hepburn, and P. L. Houston, J. Phys. Chem. **89**, 3609 (1985).
[23] N. Sivakumar, G. E. Hall, P. L. Houston, J. W. Hepburn, and I. Burak, J. Chem. Phys. **88**, 3692 (1988).
[24] C. E. Strauss, P. L. Houston, I. Burak, and J. W. Hepburn, in preparation.
[25] K. S. Sidhu, I. G. Csizmadia, O. P. Strausz, and H. E. Gunning, J. Am. Chem. Soc. **88**, 2412 (1966).
[26] W. H. Breckenridge and H. Taube, J. Chem. Phys. **52**, 1713 (1970); **53**, 1750 (1970).

[27]B. M. Ferro and B. G. Reuben, Farad. Soc. Trans. **67**, 2847 (1971).
[28]J. A. Joens, J. Phys. Chem. **89**, 5366 (1985).
[29]P. F. Zittel and L. A. Darnton, J. Chem. Phys. **77**, 3464 (1982).
[30]P. F. Zittel, L. A. Darnton, and D. D. Little, J. Chem. Phys. **79**, 5991 (1983).
[31]N. Van Veen, P. Brewer, P. Das, and R. Bersohn, J. Chem. Phys. **79**, 4295 (1983).
[32]G. Black. R. L. Sharpless, T. G. Slanger, and D. C. Lorents, J. Chem. Phys. **62**, 4274 (1975).
[33]G. Black and R. L. Sharpless, J. Chem. Phys. **70**, 5567 (1979).
[34]G. S. Ondrey, S. Kanfer, and R. Bersohn, J. Chem. Phys. **79**, 179 (1983).
[35]M. R. Taherian and T. G. Slanger, J. Chem. Phys. **81**, 3796 (1984).
[36]M. R. Taherian and T. G. Slanger, in *Photophysics and Photochemistry Above 6 eV* (Elsevier, New York, 1985).
[37]W. L. Weise, M. W. Smith, and B. M. Miles, Natl. Stand. Ref. Data Ser. Natl. Bur. Stand. **22**, 134 (1969).
[38]M. Maeda and B. P. Stoicheff, *Proceedings of the Second Topical Meeting on Laser Techniques in the Extreme Ultraviolet*, Boulder, Colorado, edited by S. E. Harris and T. B. Lucatorto, eds., (AIP Conf. Proc. No. 119) (American Institute of Physics, New York, 1984).
[39]G. Herzberg, *Molecular Spectra and Molecular Structure II. Infrared and Raman Spectra* (Van Nostrand, Princeton, NJ, 1966), p. 173.
[40]M. D. Morse and K. F. Freed, J. Chem. Phys. **74**, 4395 (1981).
[41]R. Schinke, J. Phys. Chem. **90**, 1742 (1986).
[42]R. Schinke, J. Chem. Phys. **85**, 5049 (1986).
[43]R. Schinke and V. Engel, J. Chem. Phys. **83**, 5068 (1985).
[44]W. J. Marinelli, N. Sivakumar, and P. L. Houston, J. Phys. Chem. **88**, 6685 (1984).
[45]R. D. Levine and R. B. Bernstein, *Molecular Reaction Dynamics and Chemical Reactivity* (Oxford University Press, New York, 1987), p 275.
[46]E. Zamir, R. D. Levine, and R. B. Bernstein, Chem. Phys. Lett. **107**, 217 (1984).
[47]M. I. McCarthy and V. Vaida, J. Phys. Chem. **92**, 5879 (1988).
[48]R. T Pack, J. Chem. Phys. **65**, 4765 (1976).